The International Journal of Advanced Manufacturing Technology
https://doi.org/10.1007/s00170-024-14343-8

ORIGINAL ARTICLE

Tensile properties of 3D-printed PLA prismatic cellular structures: an experimental investigation

Hashim Khan[1] · Muftooh ur Rehman Siddiqi[2] · Saim Saher[3] · Muhammad Riaz[4] · Muhammad Saad Rehan[5]

Received: 10 June 2024 / Accepted: 26 August 2024

Abstract

Advancements in additive manufacturing have significantly increased the use of cellular structures in product development, especially in the automotive, aerospace, and biomedical industries, due to their enhanced strength-to-weight ratio and energy-absorbing capabilities. This study investigates the tensile properties of 3D-printed PLA prismatic cellular structures, focusing on the effects of fillet radius, wall thickness, and cell size on tensile strength, Young's modulus, and strength-to-weight ratio. Using a full factorial design and ANOVA, we examined the impact and interaction of each geometrical parameter. Our findings show that triangular cellular structures exhibit a higher stiffness of 1.36 GPa and tensile strength of 24.28 MPa, resulting in a notable 5.78 MPa/gram strength-to-weight ratio. Increasing cell count and wall thickness enhances both tensile strength and Young's modulus, whereas adding fillet radii at corners reduces these properties. Fracture behaviors are influenced by geometrical design: shorter, thicker walls lead to progressive crack propagation, while longer, thinner walls tend to fail catastrophically. Fillet radius introduction shifts the fracture initiation point from the nodes. ANOVA results indicate that wall thickness and cell size significantly affect tensile strength and Young's modulus, contributing 36.53% and 53.54%, respectively.

Keywords Cellular structure · Additive manufacturing · Cell size · Wall thickness · Fillet radius · Strength-to-weight ratio

✉ Muftooh ur Rehman Siddiqi
m.siddiqi5@aston.ac.uk

Hashim Khan
hashimkhan@cecos.edu.pk

Saim Saher
engrsaim@gmail.com

Muhammad Riaz
rmuhammad@uob.edu.bh

Muhammad Saad Rehan
saad.rehan@uetpeshawar.edu.pk

1 Mechanical Engineering Department, CECOS University of IT & Emerging Sciences, Peshawar, Pakistan

2 Mechanical, Biomedical and Design Engineering, Aston University, Birmingham B4 7ET, UK

3 Advanced Materials Laboratory (AML), Ariston Energy Solutions, Peshawar, Pakistan

4 Mechanical Engineering Department, College of Engineering, University of Bahrain, Isa Town, Bahrain

5 U.S.-Pakistan Center for Advanced Studies in Energy, University of Engineering and Technology, Peshawar, Pakistan

1 Introduction

In recent years, the advancements in additive manufacturing (AM) technologies have significantly increased their applications in functional manufacturing [1–3]. AM offers the advantage of creating complex structures without geometric restrictions, leading to the development of lattice structures and eliminating constraints present in conventional manufacturing methods like machining and injection molding [4, 5]. A cellular structure is a porous arrangement formed by organizing unit cells, and the patterns in this structure have a significant impact on its mechanical properties. In comparison to solid structures, cellular structures present comparatively excellent prospects for creating structure that are both light weight and durable [6–9]. These structures have received substantial interest in several engineering sectors, including automobiles, aerospace, and biomedicine, due to their excellent physical and mechanical properties, leveraging additive manufacturing to create lightweight cellular structures allows for improved performance and customization in aerospace parts while reducing manufacturing costs and waste [10, 11]. Moreover, a study anticipates that the AM sector would generate $2 trillion in components and final products by 2030 [12]. Scientists are increasingly focusing on cellular structures for sustainable product development due to their lightweight, high energy absorption capability, and enhanced strength-to-weight ratio [13–15]. Huang et al. found that topology-optimized AM parts used 35–65% less material than traditional aerospace parts [16]. Given these attributes, cellular structures could be used in prostheses for children with special needs, helping them feel more confident with their limb differences and boosting self-esteem. Furthermore, cellular structures are utilized in thermal management and heat exchanger applications, including aircraft, industrial facilities, electronics cooling, and precision manufacturing. They enhance performance, energy efficiency, and reduce costs, contributing to the United Nations Sustainable Development Goals for poverty reduction and environmental protection [17]. Researchers have thoroughly investigated the printing parameters and mechanical properties of 3D-printed specimens [18]. Dong et al. found that printed PLA components depend on factors like layer thickness, raster angle, and build orientation [19]. Sajjad et al. comprehensively investigated process parameters to enhance tensile strength, recommending maintaining a lower layer thickness and printing the model parallel to the build platform [20]. Veeman et al.'s research reveals that infill density, layer thickness, and printing temperature are the most influential parameters for tensile strength/density in lattice structure optimization [21].

For structural applications, additive-manufactured polymer components are in demand. Lattice structures significantly influence the strength and mechanical properties of 3D-printed polymers. Additionally, the mechanism and failure modes of different lattice configurations should be varied and investigated experimentally. Academic studies have analyzed the mechanical properties of various lattice structures, such as Young's modulus, tensile strength, yield strength, and failure characteristics [22–24]. The stiffness and energy absorption of lattice structures are mediated by the relative density, local topology of the unit cell, stacking process, and cell size [25]. The density of cellular structures influences their mechanical properties, with higher densities resulting in greater strength. Design principles include stretch-dominated and bending-dominated types [26]. The effects of tandem, hierarchical, filled-type, negative Poisson's ratio, and embedded honeycombs on mechanical performance have been studied extensively [27]. Plenty of researchers have undertaken substantial research on honeycomb constructions made of metal components [28–31]. Despite substantial research on metal honeycomb constructions, there have been fewer studies on the use of polymers [32], ceramics [33], and carbon fiber–reinforced polymers in additive manufacturing [34]. Amirkhani et al. studied the scaffold failure mechanism and found that cubic unit cells and nodal connectivity of 3 and 4 evoke elastic–plastic deformation, while trigonal unit cells 4 and 6 are brittle [35]. Geng et al. found progressive fracture propagation in rhombic dodecahedron lattice structures and catastrophic fracture patterns in body-centered cubic structures under quasi-static tensile load [36]. Nadir et al. revealed that gyroid structures with 2 mm or greater surface layers improve mechanical properties [37]. Davis et al. observed that honeycomb lattice structural strength deviates 7% from scanned geometry predictions [38]. Nikolaos et al. found that an increase in aspect ratio significantly impacts the mechanical properties of various strut-lattice structures [39]. Fleck et al. found that Kagome lattice has higher fracture toughness due to an elastic zone, while hexagonal and triangular honeycombs are flaw-sensitive [40]. Li et al. found that constrained sandwich panels increase elastic modulus by 1.5 times, emphasizing the importance of considering mechanical properties rather than individual cellular core predictions [41]. Maskery et al. found that cell size significantly influences the failure mechanism of metal lattices of double-gyroid cellular structures [42]. Recent research on the behavior of lattice structures during buckling and post-buckling showed that the lattice unit cell fails at the corner due to residual stresses at sharp corners [43–45]. Latture et al. found that the presence of fillets at nodes in an additively manufactured octet truss increased the peak stress by 20% [46]. Chuang et al. reported a strong correlation between hexagonal honeycomb relative density and elastic buckling strength. Lower density levels increased honeycomb strength marginally, while higher density levels raised its strength [47]. Simone and Gibson's finite element analysis revealed that the stiffness and strength of hexagonal honeycombs initially increase with increasing solid distribution at vertices [48]. Li et al. discovered that 2D bending-dominated structures show progressive crack propagation, while 2D stretching-dominated structures show catastrophic brittle fracture failure, with higher energy absorption [49]. Khosravani et al. have effectively demonstrated the impact of post-processing and thermal aging on the structural integrity of both intact and defected 3D-printed polymer specimens [50–52]. Additionally, Khan et al. extensively investigated the effects of various processing parameters on the fracture toughness of 3D-printed composite structures. These parameters include printing temperature, printing speed, layer thickness, and nozzle geometries. Other crucial factors influencing the fracture properties of printed parts, such as surface treatment, annealing, and porosity, were also examined and reported [53]. Lyu and Lu demonstrated that applying a coating to 3D-printed parts enhances certain mechanical characteristics [54].

Reviewing the extant literature, most studies have analyzed cell size, relative density, wall thickness, fillet radius, and topology under compression tests. However, the mechanical behavior of prismatic cellular structures—such as triangular, hexagonal, and octagonal structures—with various geometrical parameters under tensile loading remains underexplored. Therefore, a thorough investigation is imperative to carefully examine the geometrical parameters, such as cell size, wall thickness, and fillet radius, aiming to comprehend the mechanical behavior of polymeric materials in conjunction with these geometrical parameters. This study aims to understand the impact of these design parameters on tensile strength, Young's modulus, and fracture failure behavior. Initially, the present investigation entailed the experimental examination of three unique cellular structures with identical geometrical parameters under quasi-static tensile loading. Based on initial results, the structure with the highest strength-to-weight ratio and stiffness was selected for a detailed examination of mechanical response under tensile loading for a set of geometrical parameters. A full factorial design of experiments was conducted to delve into the response and contribution of each input parameter to mechanical behavior such as Young's modulus and tensile strength. This comprehensive analysis provides a novel perspective on the effect of cell size, wall thickness, and fillet radius on different aspects of cellular mechanical behavior. This investigation brings a new dimension to our understanding of lattice structures, with implications for diverse applications within engineering and design.

2 Materials and methods

To identify the mechanical properties of cellular structures, a collection of specimens with distinctive shapes was printed using fused deposition modeling technology to conduct tensile tests. In the current study context, a wide variety of specimens were printed by melting a 1.75-mm diameter PLA filament through a nozzle of 0.4-mm diameter. These specimens were designed using PTC Creo 8.01 following ASTM D638-14 Type-I [55] standards, as shown in Fig. 1a. The CAD geometry was translated into G-Codes using Cura 5.30, an open-source software. A full factorial DOE was conducted to examine the effects of geometrical parameters (cell size/wall length, wall thickness, and fillet radius). Parameters were evaluated at three levels: cell size (6 to 16 mm), wall thickness (0.5 to 1.75 mm), and fillet radius (0.00, 0.35, and 0.85 mm). A study analyzed the effects of parameters on triangular cell structures, and the results were carefully examined. Each component was printed individually in a randomized sequence using Minitab software, which was also utilized for statistical analysis after the experiment. The specimens were produced using an open-source printer.

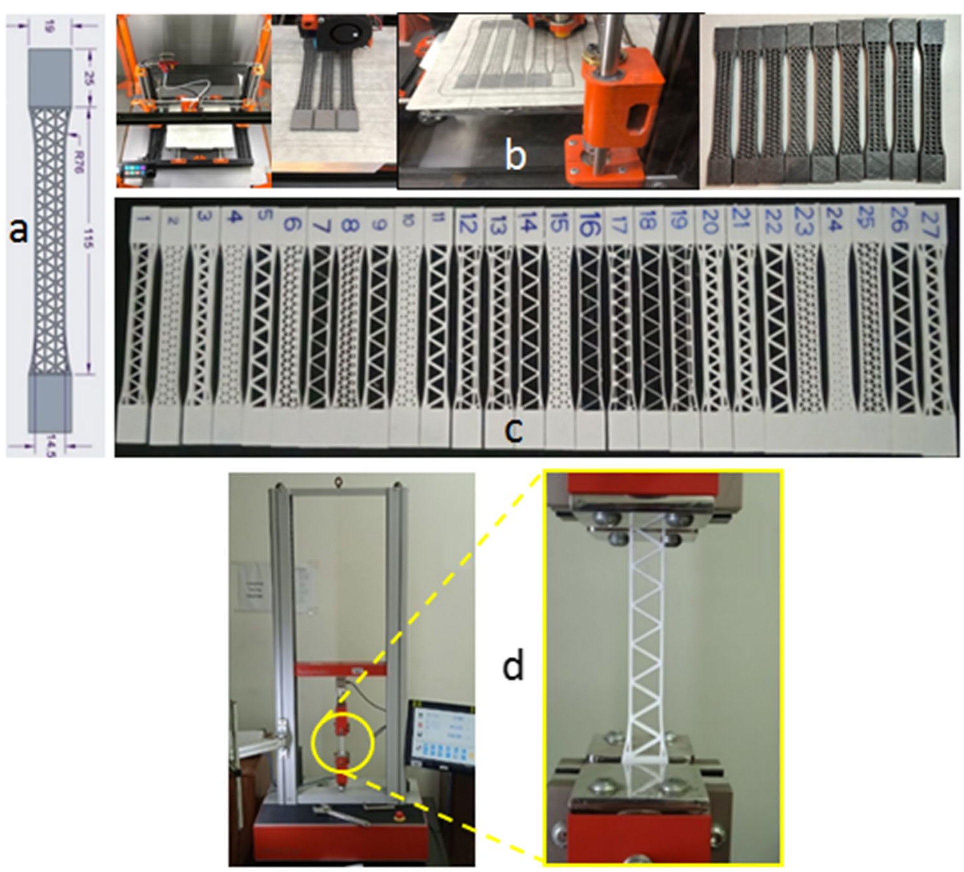

Fig. 1 **a** Cellular Structure CAD Model, **b** 3DPrinting of specimen, **c** Printed specimens, and **d** Experimental setup loaded with specimen

Choosing the appropriate process parameters is crucial for the successful printing of load-bearing components. Research shows how these parameters affect the properties of printed materials. Tymrak et al. [56] found that a 0.2-mm thickness layer with an infill line direction of 0 and 90° can increase PLA's ultimate tensile strength (UTS). Abeykoon discovered that the optimal conditions for achieving the highest UTS in printed PLA are a temperature of 215 °C, a printing speed of 90 mm/s, and a linear pattern infill density of 100% [21, 57]. Based on these findings, it is crucial to conduct further research on the mechanical behavior of additively manufactured lattice structures in relation to their various geometrical parameters. This will ensure a more comprehensive understanding of the cellular structure under different geometrical parameters.

A summary of the materials and printing process parameters can be found in Table 1. The measurement of the specimens' weight was conducted after the printing process and the subsequent elimination of the support layers. To accurately analyze the geometric parameters, the specimens underwent a tensile examination following the guidelines set by the ASTM D638-14 [55] standards. Figure 1c depicts the Testo Metric M500-30AT 30kN loading frame system equipped with a 5kN load cell, which applied a constant displacement rate of 1 mm/min until failure was attained. These testing methods align with the requirements outlined in ASTM standard D638 [55], offering dependable and precise data for academic analysis. All tests were conducted at ambient temperature. The experimental data for engineering strain and engineering stress have been reported. Prior to testing, the cross-sectional area of the gauge region was calculated using a digital caliper. Engineering stress–strain curves were used to calculate Young's modulus, effective tensile strength, and strength-to-weight ratio.

Table 1 Sets of used process parameters

Description	Parameters
Material	PLA
Layer height (mm)	0.2
Wall line count	2
Top/Bottom thickness (mm)	1
Top/Bottom layer (mm)	2
Infill density	100%
Infill pattern	Line
Infill line direction	0, 90
Infill layer thickness (mm)	0.2
Printing temperature (°C)	215
Build pate temperature (°C)	60
Print speed (mm/s)	90
Retraction distance (mm)	5
Retraction speed (mm/s)	45

3 Results and discussion

3.1 Cellular patterns mechanical behavior under tension

The specimens were investigated under quasi-static loading guidelines compliant with ASTM [43, 55] standards for tensile tests. The stress–strain curves for the distinct cellular patterns, all with the same relative density of 28%, along with the solid specimen, are presented in Fig. 2. Upon initial loading, both the cellular structure and solid specimens exhibited elastic behavior, transitioning from the elastic to the plastic region beyond the peak point.

As shown in Table 2, the triangular cellular structure possesses a Young's modulus of 1.36 GPa, a tensile strength of 24.28 MPa, and a strength-to-weight ratio of 5.78 MPa/gram, which are notably higher than those of the hexagonal and octagonal cellular structures. This cellular structure underwent distinct mechanical behavior classified by Ashby [26]. The hexagonal and octagonal cellular patterns yield a bending-dominant behavior, whereas the triangular cellular structure results in stretch-dominant behavior. Upon loading, the hexagonal and octagonal structure walls experience a maximum moment at the junction points, causing the walls to bend. In contrast, the triangular structure's struts parallel to the loading direction support axial force in both tensile and compressive manners, resulting in stretching-dominant deformation [58]. It is evident from Fig. 2 that the maximum strain of 3.5% is recorded for hexagonal structures. Beyond the yield point, plastic hinge formation occurs at the section's maximum bending moment,

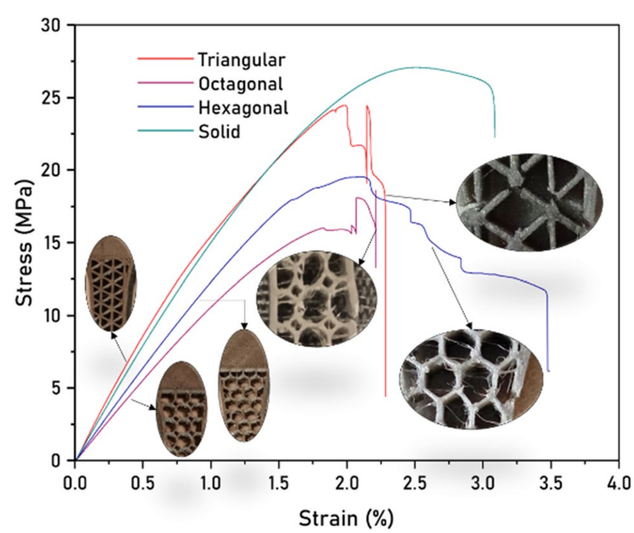

Fig. 2 Stress strain plots of three different cellular structures along with solid specimen

Table 2 Mechanical behavior of distinct lattice structure and solid specimen under tensile test

S.no	Type of lattice structure	Tensile strength (MPa)	Strength to weight ratio (MPa/gram)	Young's modulus (GPa)
1	Triangular	24.28	5.78	1.36
2	Hexagonal	19.542	5.07	1.26
3	Octagonal	15.911	4.07	1.1
4	Solid specimen	27	3.176	1.63

allowing significant strain. However, the walls parallel to the loading direction resist deformation in triangular cells, allowing minimal deformation at the junction point, resulting in higher stiffness and tensile stresses. These experimental findings align with the literature presented by Wu et al. [49]. Initial failure in the lattice structure was observed to occur at the outer walls, propagating towards the interior structure. Upon initial failure, the failed wall no longer contributes to the load-bearing capacity of the structures, and the stresses in the remaining lattice structure are redistributed. This leads to sawtooth-like patterns in each stress–strain curve, more prominent in hexagonal structures than in any other structure. Further increasing the load causes additional walls within the structure to fail. This progressive failure process continues until the complete failure of the entire structure occurs. Moreover, stretch-dominant and bending-dominant structure failure mechanisms are distinct under tension. Upon loading, the triangular cell's slanted walls experience compression, while the walls parallel to the loading direction experience tension. At the junction point, the walls experience a moment where stress reaches a critical level, causing a fracture. Bending-dominant structures, upon initial loading, give a linear elastic curve, and beyond the yield point, plastic hinge formation occurs at the junction where maximum bending occurs, allowing significant deformation. This causes one of the walls parallel to the loading direction to stretch and eventually fracture. Stretch-dominant structures resist deformation, rupturing abruptly with minimal deformation [25].

3.2 Effect of cell size fillet radius and wall thickness on tensile strength and Young's modulus

Figure 3a–c shows the tensile strength of a triangular lattice structure with varying cell sizes (wall lengths) from 6 to 16 mm and fillet radii from 0 to 0.85 mm. The wall thickness for each in Fig. 3a–c represents 0.5 mm, 1.1 mm, and 1.75 mm, respectively. A consistent decreasing trend in tensile strength is observed as the wall length increases from 6 to 16 mm, regardless of wall thickness.

In Fig. 3a, increasing the wall length from 6 to 16 mm reduces the tensile strength. This is because, upon loading, the triangular structure fractures at the junction due to moments. Gibson and Ashby [25] stated that the moment is directly proportional to the applied load and wall length. When the wall length increases, the moment rises, causing fractures at a lower force compared to shorter walls. Adding and increasing the fillet radius to 0.5 mm walls boosts the tensile strength for all cell sizes. Figure 3b shows that increasing wall thickness to 1.10 mm significantly enhances the tensile strength for each wall length or cell size. These experimental findings align with results reported in the literature by Yan Wu [49]. Furthermore, in Fig. 3b, incorporating a fillet radius to the 6-mm cell size raises the tensile strength, but further increasing the fillet radius to 0.85 mm has no substantial impact. For larger 11 mm and 16-mm cell sizes, increasing the fillet radius to 0.85 mm results in a marginal decline in tensile strength. Figure 3c indicates that tensile strength is comparatively higher for wall thicknesses beyond 1.75 mm. However, adding fillets to the cell walls significantly decreases tensile strength, and this trend

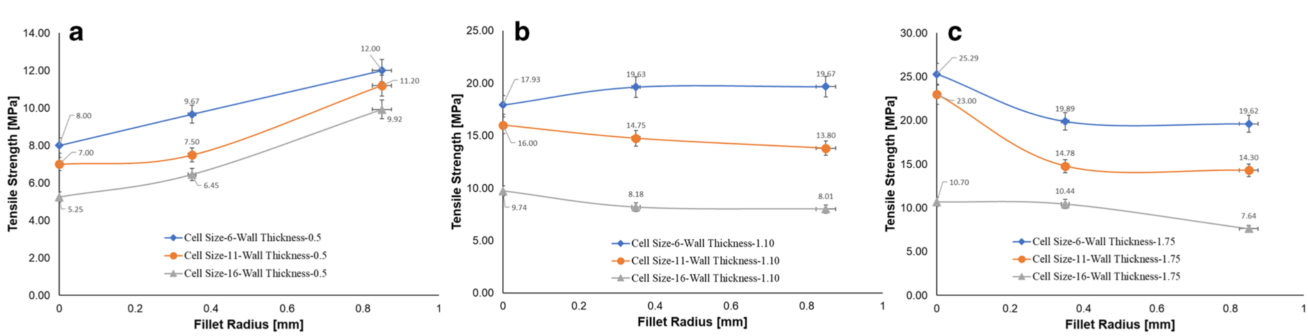

Fig. 3 Influence of various cell size, wall thickness and fillet radius on tensile strength

is consistent across all cell sizes. This is because adding and increasing the fillet radius at the nodes distributes material, weakening other regions of the cellular walls and reducing tensile strength, especially in shorter and thicker walls [59].

Figure 4a–c shows the effective Young's modulus against varying wall lengths or cell sizes (6 to 16 mm) and fillet radii (0 to 0.85 mm). The wall thickness is kept constant in each Fig. 4. Increasing the cell size from 6 to 16 mm substantially decreases stiffness across all wall thickness levels. However, increasing wall thickness from 0.5 to 1.75 mm for 6 mm and 11-mm cell sizes significantly boosts Young's modulus. This is because lower cell sizes increase the cell count, thereby increasing resistance to deformation. On the other hand, increasing wall thickness beyond 1.10 mm for 16-mm wall lengths results in only a marginal change in stiffness. Increasing the fillet radius from 0 to 0.85 mm reveals a significant decline in Young's modulus, especially when wall thickness exceeds 1.10 mm. Adding fillets to the vertex of the cell adds material to the area, but the mid-region of the wall becomes shorter in width compared to the corner section, weakening the mid-region. This phenomenon is more prominent in thicker (1.75 mm) and shorter wall lengths or cell sizes.

From the above discussion, it can be inferred that the fillet radius might not adequately cover the wall junctions for larger 16-mm cell sizes as effectively as it does for smaller 6-mm cell sizes. Therefore, establishing a dimensionless number is imperative to predict the mechanical behavior for larger cell sizes.

3.3 Effect of cell size wall thickness and fillet radius on strength-to-weight ratio

Figure 5a presents the strength-to-weight ratio for a 6-mm cell size with varying wall thicknesses from 0.5 to 1.75 mm and fillet radii from 0 to 0.85 mm. It is evident that without varying the fillet radius, increasing the wall thickness from 0.5 to 1.75 mm results in a significant boost in the strength-to-weight ratio. Additionally, incorporating a fillet radius and increasing the wall thickness initially enhances the strength-to-weight ratio. However, increasing the wall thickness beyond 1.10 mm decreases the strength-to-weight ratio. Notably, increasing the fillet radius to 0.85 mm for the 0.5-mm thinner walls enhances the strength-to-weight ratio, but further increasing the wall thickness beyond 1.10 mm leads to a decline. The reason is that shorter, thicker walls with a higher fillet radius shorten the mid-region, reducing the strength-to-weight ratio.

Figure 5b shows the strength-to-weight ratio for an 11-mm cell size with varying wall thicknesses from 0.5 to 1.75 mm and fillet radii from 0 to 0.85 mm. It is important to note that increasing the wall thickness without a fillet radius

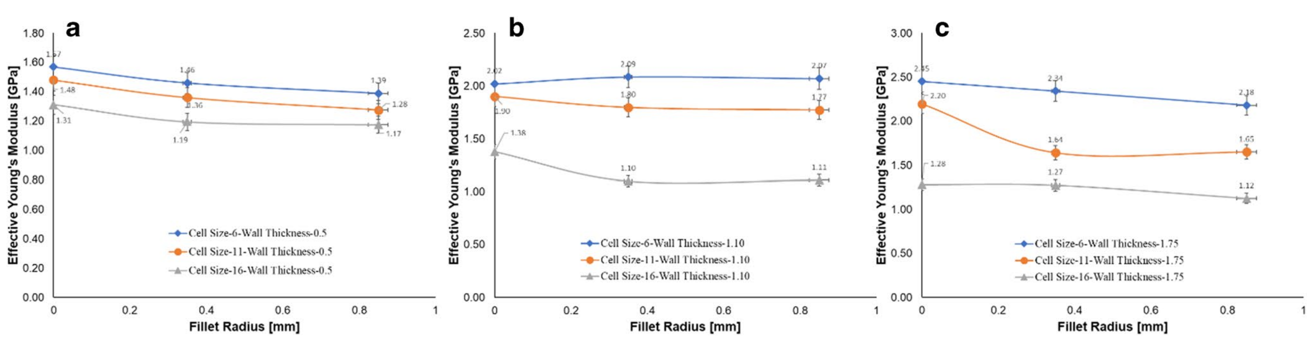

Fig. 4 Impact of cell size, wall thickness and fillet radius on effective Young's modulus

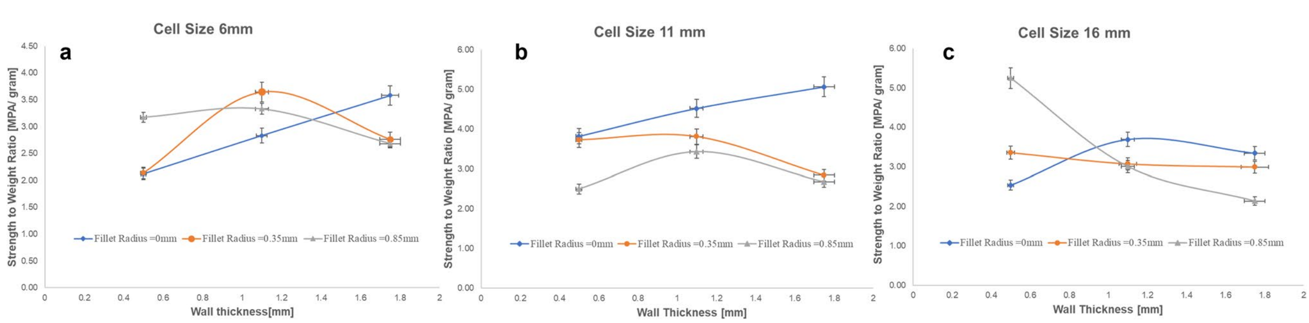

Fig. 5 Various geometrical parameters impact on its strenght-to-weight ratio

enhances the strength-to-weight ratio. Moreover, adding a fillet radius of 0.35 mm to a 0.5-mm thinner wall does not significantly affect the strength-to-weight ratio. However, further increasing the fillet radius to 0.85 mm results in a decline, especially noticeable in 1.75-mm thicker walls.

Figure 5c depicts the strength-to-weight ratio for a 16-mm cell size with varying wall thicknesses from 0.5 to 1.75 mm and fillet radii from 0 to 0.85 mm. Varying the wall thickness from 0.5 to 1.10 mm without a fillet radius enhances the strength-to-weight ratio. However, there is a marginal decline when the wall thickness reaches 1.75 mm. Incorporating a 0.35-mm fillet radius and increasing the wall thickness from 0.5 to 1.75 mm yields no substantial enhancement in the strength-to-weight ratio. Further increasing the fillet radius to 0.85 mm with varying wall thickness from 0.5 to 1.75 mm significantly declines the strength-to-weight ratio.

3.4 Macroscopic failure analysis of tested specimens

The fractured specimens under tensile tests with distinct geometrical parameters are shown in Fig. 6. Generally, upon loading, the specimen initially exhibits elastic behavior, followed by plastic deformation, and ultimately experiences brittle fracture. The fracture typically begins at the outer walls and propagates towards the internal cellular structures, as previously observed by Palaniyappan [21].

Figure 6 clearly shows that in thinner walls (0.5 mm) for all cell sizes, fractures occur at the junctions of the structure, indicating that wall failure is primarily due to bending moments followed by stretching, as shown by the green and red arrows, respectively. This is because thinner walls (0.5 mm) primarily resist stretching but not bending. Consequently, fractures due to bending moments occur at lower levels. Under tension, each cell experiences tension and compression in their walls and bending moments at the junction points. The crack pattern propagation depends on the geometrical design parameters, with cracks initiating from the outer walls and moving towards the interior structures, implying that crack propagation depends on wall thickness [49] and wall length.

Increasing the wall thickness beyond 1.10 mm for all cell sizes results in fractures due to stretching more prominently than bending moments, with the red arrows indicating that rupture occurs parallel to the loading direction. Notably, increasing the wall thickness boosts the plastic deformation zone, as thicker walls allow for large deformations due to plastic hinge formation after the peak point.

Adding a fillet radius to the junction points shifts the rupture point from the junction to other regions, independent of wall length and thickness [59]. It is also noteworthy that a higher number of cells exhibit a more consistent fracture pattern, which becomes more consistent as the strut thickness increases. In contrast, a lower number of cells tend to exhibit catastrophic failure of the structures [49].

3.5 Statistical analysis

The statistical analysis technique of Analysis of Variance (ANOVA) was employed to ascertain the impact of geometrical parameters on measured mechanical properties. ANOVA is a powerful tool that assesses the influence of independent variables on a dependent variable by comparing the distribution of populations in a dataset. It determines the extent to which the independent variables, or factors,

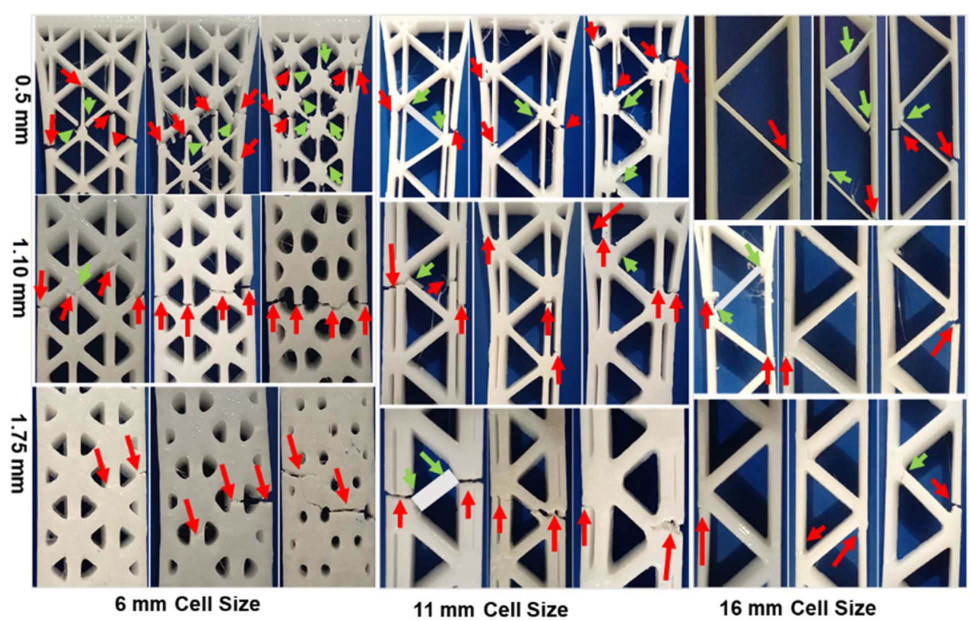

Fig. 6 Macroscopic failure analysis of distinct geometrical parameters cellular structures

influence the output values or dependent variable. Each group within a factor is referred to as a level [60].

The variables chosen for this investigation were Cell size, Wall thickness, and Fillet radius, based on their potential to significantly alter tensile strength and effective Young's modulus. The variation in cell size is expected to have a significant impact on mechanical properties, making it an important consideration. The wall thickness was also examined due to its potential effect on mechanical behavior. Finally, the fillet radius, or material distribution at nodes, was included in the analysis if it showed potential for improving mechanical behavior.

The statistical software Minitab was used to conduct the ANOVA, with a confidence level of 95% chosen for the analysis. From ANOVA *P*-value less than 0.05, statistical significance was determined. The ANOVA results are presented in Table 3, accompanied by a Pareto chart of standardized effects for effective Young's modulus and tensile strength, as depicted in Fig. 7. These charts offer a valuable means of comprehending the relative impact of each input variable by providing a dimensionless representation of their magnitude and significance [60].

From Fig. 7a, it is apparent that cell size, wall thickness, fillet radius, and the interaction between cell size and wall thickness exceed the 2.31 critical standard value, represented by a vertical dashed line on the Pareto chart, implying that these parameters have a significant statistical impact on effective Young's modulus. Similarly, Fig. 7b illustrates that cell size, wall thickness, fillet radius, and interactions between factors such as cell size and wall thickness, and fillet radius and wall thickness, surpass the 2.306 critical standard value, indicating a statistically significant influence on tensile strength.

On the other hand, it is noteworthy that the interaction between cell size and fillet radius is statistically insignificant for both Young's modulus and tensile strength. Additionally, the interaction between wall thickness and fillet radius is insignificant only for Young's modulus. Furthermore, fillet radius has no statistically substantial impact on tensile strength.

The main effects charts for Young's modulus and tensile strength are shown in Fig. 8, respectively. It has been shown that increasing wall thickness significantly increases tensile strength, most likely because more material is available to withstand applied stresses. In contrast, increasing cell size lowers tensile strength, presumably due to lower material density. Tensile strength declines with increasing fillet radius, possibly because the stress concentration reduction effect becomes less relevant as the fillet radius grows. Thicker walls provide better resistance to deformation,

Table 3 ANOVA analysis of each factor and level

Sources	DF	Tensile strength			Effective Young's modulus		
		Contribution	*F*-value	*P*-value	Contribution	*F*-value	*P*-value
Wall thickness	2	36.53%	35.71	0.000	21.02%	32.65	0.00014
Cell size	2	31.28%	30.58	0.000	53.54%	83.17	0.00000
Fillet radius	2	2.26%	2.21	0.172	4.92%	7.64	0.01395
Wall thickness*Cell size	4	10.86%	0.000	0.022	15.33%	11.91	0.00189
Wall thickness*Fillet radius	4	9.03%	0.000	0.035	1.19%	0.93	0.49459
Cell size*Fillet radius	4	5.95%	0.172	0.093	1.43%	1.11	0.41424
Error	8	4.09%	-	-	-	-	-
Total	26	100.00%	-	-	-	-	-

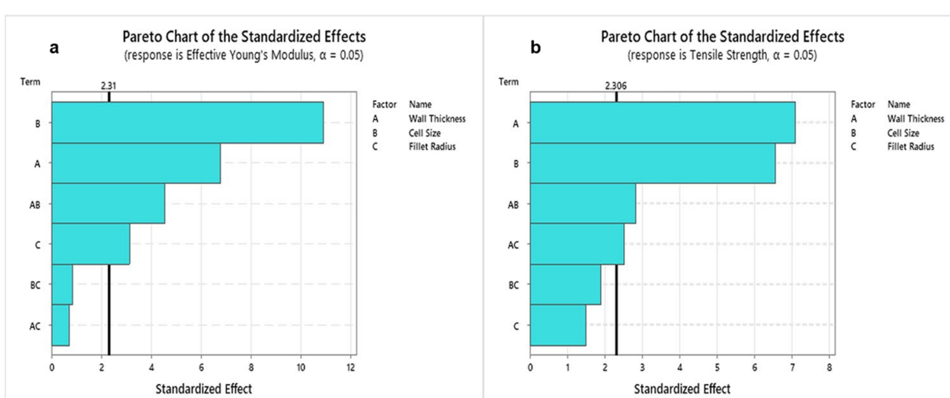

Fig. 7 Pareto charts for effective young's modulus & tensile strength

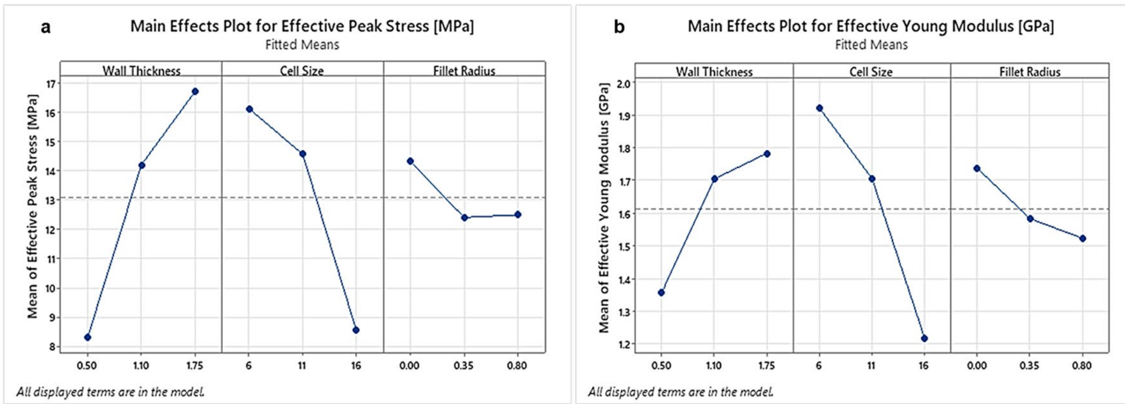

Fig. 8 Main effect plots of tensile strength and young's modulus

which significantly enhances stiffness for effective Young's modulus (Fig. 8b). However, beyond 1.10-mm thickness the difference is minimum. Young's modulus decreases when cell walls lengthen (cell size increases), perhaps leading to more flexible materials. Increasing fillet radius reduces stiffness, possibly due to less effective stress distribution within the material. Figure 8b depicts the main effects plots for the effective Young's modulus. Thicker walls are more resistant to deformation, hence increasing their thickness significantly enhances stiffness. Lengthening cell walls (raising cell size) lowers Young's modulus, perhaps leading to more flexible structures. Increasing the fillet radius affects stiffness, potentially due to less effective stress distribution inside the material.

Table 3 provides the results of the ANOVA analysis for both tensile strength and effective Young's modulus. It becomes clear from the table that wall thickness contributes 36.53% and has utmost significance for tensile strength, while cell size plays a pivotal role with a contribution of 53% for effective Young's modulus. Additionally, a *P*-value of less than 0.05 is deemed statistically significant, while values higher than this are considered insignificant.

Figure 8 depicts the main effects plots for tensile strength and effective Young's modulus. It can be inferred that the mean tensile stress or peak stress is significantly boosted by increasing wall thickness. On the other hand, varying cell size or wall length reduces these properties. Moreover, adding and increasing fillet radius to tensile strength and effective Young's modulus yields a decline in these mechanical behaviors.

To validate the ANOVA results, a regression equation for tensile strength was developed in Eq. (1) with an adjusted coefficient of determination of 95.91%. To validate the predictive ability of the models, the predicted tensile strength was compared to the corresponding experimental values, as depicted in Fig. 9 demonstrating strong agreement between predicted and experimental values. The minimal differences between predicted and experimental values validate the models' predictive ability, thereby confirming the ANOVA results.

$$\begin{aligned}\text{Tensile Strength} = & -0.52 + 19.69\ \text{Wall Thickness} + 0.260\ \text{Cell Size} \\ & - 0.849\ \text{Wall Thickness} \times \text{Cell Size} + 10.50\ \text{Fillet Radius} \\ & - 9.48\ \text{Fillet Radius} \times \text{Wall Thickness}\end{aligned} \tag{1}$$

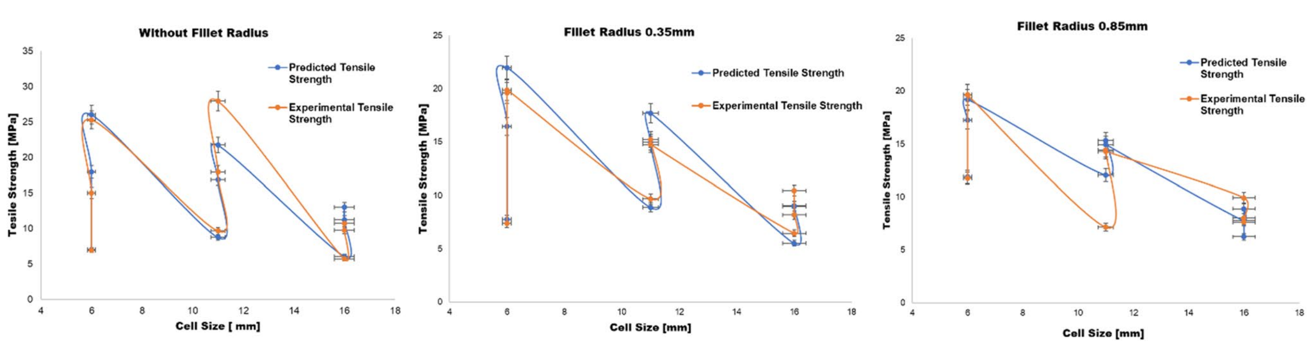

Fig. 9 Experimental and predicted values for the tensile strength

The standard deviation, a critical statistical measure of dispersion, provides insight into the consistency and reliability of the tensile strength, Young's modulus, and other mechanical properties evaluated in this study. Throughout the experiments, the standard deviations of the measured properties were consistently within acceptable limits, indicating a high degree of repeatability and precision in the results. This adherence to low standard deviation highlights the robustness of the experimental procedures and the reliability of the data presented. Additionally, the potential for error in calculations was meticulously accounted for in the analysis. Error margins were minimized through rigorous methodological approaches, including precise calibration of testing equipment and adherence to standardized measurement protocols. The error analysis, therefore, demonstrates that the deviations from the calculated values are minimal, reinforcing the accuracy and validity of the results. The careful consideration of these factors ensures that the conclusions drawn from the data are based on robust and reliable measurements, enhancing the credibility of the findings and their implications for the field of additive manufacturing.

4 Conclusion

The study highlights the increasing significance of cellular structures in additive manufacturing, particularly for industries such as automotive, aerospace, and biomedical, due to their enhanced strength-to-weight ratios and energy absorption capabilities. This research into 3D-printed PLA prismatic cellular structures demonstrates that triangular geometries achieve the highest tensile strength (24.28 MPa), stiffness (1.36 GPa), and strength-to-weight ratio (5.78 MPa/gram) compared to other shapes. The findings reveal that increasing cell count and wall thickness generally improves tensile strength and Young's modulus. However, adding fillet radii at corners tends to decrease these properties for thicker walls. Fracture behavior is influenced by the geometry: thicker walls with shorter cell sizes show progressive crack propagation, while thinner walls with longer cells tend to fail catastrophically. The introduction of fillet radii shifts the point of fracture initiation away from the nodes. ANOVA analysis confirms that wall thickness and cell size have significant effects on tensile strength and Young's modulus, with contributions of 36.53% and 53.54%, respectively. Optimizing geometrical parameters such as wall thickness and cell size is crucial for enhancing mechanical properties. The insights gained from this study offer valuable guidance for designing cellular structures that perform better and contribute to the sustainability of additive manufacturing practices influencing UN SDG 9, 12 and 13.

Author contribution Conceptualization, Muftooh Siddiqi; Data curation, Hashim Khan. and Muftooh Siddiqi.; Formal analysis, Hashim Khan, Muftooh Siddiqi, Saim Saher and Muhammad Riaz.; Funding acquisition, Muftooh Siddiqi.; Investigation, Hashim Khan, Muftooh Siddiqi Saim Saher and Muhammad Riaz Methodology, Muftooh Siddiqi.; Software, Hashim Khan and Muhammad Riaz. and M.S.R.; Experimentation: Muhammad Saad Rehan and Hashim Khan; Supervision, Muftooh Siddiqi and Saim Saher; Validation, Hashim Khan, Muhammad Riaz and Muhammad Saad Rehan.; Visualization, Hashim Khan, Saim Saher and Muhammad Riaz; Writing—original draft, Hashim Khan, Muftooh Siddiqi, Saim Saher and Muhammad Riaz; Writing—review & editing, Saim Saher., Muhammad Riaz. All authors have read and agreed to the published version of the manuscript.

Declarations

Conflict of interest The authors declare no competing interests.

References

1. González-Henríquez CM, Sarabia-Vallejos MA, Rodriguez-Hernandez J (2019) Polymers for additive manufacturing and 4D-printing: materials, methodologies, and biomedical applications. Prog Polym Sci 94:57–116. https://doi.org/10.1016/j.progpolymsci.2019.03.001
2. Siddiqi MUR, Muhammad R, Xu Y, Zuhra FT, Khan NB (2024) Reverse engineering of a 6 DOF industrial robotic arm for advanced manufacturing processes. In: Integration of heterogeneous manufacturing machinery in cells and systems. CRC Press, pp 76–88. https://doi.org/10.1201/9781003376620-8
3. Siddiqi MUR, Corney JR, Sivaswamy G, Amir M, Bhattacharya R (2017) Design and validation of a fixture for positive incremental sheet forming. Proc Inst Mech Eng Part B J Eng Manuf 232(4):629–643. https://doi.org/10.1177/0954405417703423
4. Frazier WE (2014) Metal additive manufacturing: a review. J Mater Eng Perform 23(6):1917–1928. https://doi.org/10.1007/s11665-014-0958-z
5. Smart 3D Nanoprinting, fundamentals, materials, and applications. 2022. https://doi.org/10.1201/9781003189404
6. Khosroshahi SF, Tsampas SA, Galvanetto U (2018) Feasibility study on the use of a hierarchical lattice architecture for helmet liners. Mater Today Commun 14:312–323. https://doi.org/10.1016/j.mtcomm.2018.02.002
7. Wang C, Gu X, Zhu J, Zhou H, Li S, Zhang W (2020) Concurrent design of hierarchical structures with three-dimensional parameterized lattice microstructures for additive manufacturing. Struct Multidiscip Optim 61(3):869–894. https://doi.org/10.1007/s00158-019-02408-2

8. Kim H, Kim E, Yang J (2019) Nonlinear wave propagation in 3D-printed graded lattices of hollow elliptical cylinders. J Mech Phys Solids 125:774–784. https://doi.org/10.1016/j.jmps.2019.02.001
9. du Plessis A et al (2019) Beautiful and functional: a review of biomimetic design in additive manufacturing. Addit Manuf 27:408–427. https://doi.org/10.1016/j.addma.2019.03.033
10. Chu C, Graf G, Rosen DW (2008) Design for additive manufacturing of cellular structures. Comput Aided Des Appl 5:686–696
11. A Junaid et al. (2022) "Metrology process to produce high-value components and reduce waste for the fourth industrial revolution." https://doi.org/10.3390/su14127472.
12. O Paper (2023) "Additive manufacturing: expanding 3D printing horizon in industry." 2221–2235
13. Zadpoor AA (2019) Mechanical performance of additively manufactured meta-biomaterials. Acta Biomater 85:41–59. https://doi.org/10.1016/j.actbio.2018.12.038
14. Amin Yavari S et al (2015) Relationship between unit cell type and porosity and the fatigue behavior of selective laser melted meta-biomaterials. J Mech Behav Biomed Mater 43:91–100. https://doi.org/10.1016/j.jmbbm.2014.12.015
15. Zhang XZ, Leary M, Tang HP, Song T, Qian M (2018) Selective electron beam manufactured Ti-6Al-4V lattice structures for orthopedic implant applications: current status and outstanding challenges. Curr Opin Solid State Mater Sci 22(3):75–99. https://doi.org/10.1016/j.cossms.2018.05.002
16. Huang R et al (2016) Energy and emissions saving potential of additive manufacturing: the case of lightweight aircraft components. J Clean Prod 135:1559–1570. https://doi.org/10.1016/j.jclepro.2015.04.109
17. nTopology, "Guide to lattice structures in additive manufacturing," nTopology pp. 1–14, 2022, [Online]. Available: https://ntopology.com/blog/guide-to-lattice-structures-in-additive-manufacturing/
18. M Waseem et al (2020) "Multi-response optimization of tensile creep behavior of PLA 3D printed parts using categorical response surface methodology." https://doi.org/10.3390/polym12122962
19. Dong G, Wijaya G, Tang Y, Zhao YF (2018) Optimizing process parameters of fused deposition modeling by Taguchi method for the fabrication of lattice structures. Addit Manuf 19:62–72. https://doi.org/10.1016/j.addma.2017.11.004
20. Farashi S, Vafaee F (2022) Effect of printing parameters on the tensile strength of FDM 3D samples: a meta-analysis focusing on layer thickness and sample orientation. Prog Addit Manuf 7(4):565–582. https://doi.org/10.1007/s40964-021-00247-6
21. S Palaniyappan, D Veeman, S Narain Kumar, GJ Surendhar, L Natrayan (2022) "Effect of printing characteristics for the incorporation of hexagonal-shaped lattice structure on the PLA polymeric material." J Thermoplast Compos Mater 0(0):1–22. https://doi.org/10.1177/08927057221089832
22. G de NJ Rodrigo Garcia Motta, A Link, V Aparecida Bussolaro et al. (2021) "Rodrigo Garcia Motta, Angélica Link, Viviane Aparecida Bussolaro, Geraldo de Nardi Junior." Pesqui Vet Bras 26(2): 173–180 [Online]. Available: http://www.ufrgs.br/actavet/31-1/artigo552.pdf
23. Yan C, Hao L, Hussein A, Young P, Raymont D (2014) Advanced lightweight 316L stainless steel cellular lattice structures fabricated via selective laser melting. Mater Des 55:533–541. https://doi.org/10.1016/j.matdes.2013.10.027
24. Deshpande VS, Fleck NA, Ashby MF (2001) Effective properties of the octet-truss lattice material. J Mech Phys Solids 49(8):1747–1769. https://doi.org/10.1016/S0022-5096(01)00010-2
25. Lakes RS (1989) Cellular solids. J Biomech 22(4):397. https://doi.org/10.1016/0021-9290(89)90056-0
26. P T R S A (2006) "The properties of foams and lattices." 15–30. https://doi.org/10.1098/rsta.2005.1678
27. Wang Z (2019) Recent advances in novel metallic honeycomb structure. Compos Part B Eng 166(January):731–741. https://doi.org/10.1016/j.compositesb.2019.02.011
28. Zhou Z, Zhou J, Fan H (2017) Plastic analyses of thin-walled steel honeycombs with re-entrant deformation style. Mater Sci Eng A 688(C):123–133. https://doi.org/10.1016/j.msea.2017.01.056
29. G Ghongade, KP Kalyan, R Vaira Vignesh, M Govindaraju (2019) "Design, fabrication, and analysis of cost effective steel honeycomb structures." Mater Today Proc 46(xxxx):4520–4526. https://doi.org/10.1016/j.matpr.2020.09.694
30. Selivanov VV, Silnikov MV, Markov VA, Popov YV, Pusev VI (2021) Using highly porous aluminum alloys and honeycomb structures in spacecraft landing gear. Acta Astronaut 180:105–109. https://doi.org/10.1016/j.actaastro.2020.12.014
31. ZareiMahmoudabadi M, Sadighi M (2011) A study on the static and dynamic loading of the foam filled metal hexagonal honeycomb – theoretical and experimental. Mater Sci Eng A 530(Completed):333–343. https://doi.org/10.1016/j.msea.2011.09.093
32. Rowan HM, Faculty E, Rahman O (2020) Rowan Digital Works Optimization of energy absorption performance of polymer honeycombs by density gradation. Compos Part C: Open Access density gradation 3:100052
33. Hu JS, Wang BL (2021) Crack growth behavior and thermal shock resistance of ceramic sandwich structures with an auxetic honeycomb core. Compos Struct 260:113256. https://doi.org/10.1016/j.compstruct.2020.113256
34. Yan L, Zhu K, Chen N, Zheng X, Quaresimin M (2021) Energy-absorption characteristics of tube-reinforced absorbent honeycomb sandwich structure. Compos Struct 255:112946. https://doi.org/10.1016/j.compstruct.2020.112946
35. Amirkhani S, Bagheri R, ZehtabYazdi A (2012) Manipulating failure mechanism of rapid prototyped scaffolds by changing nodal connectivity and geometry of the pores. J Biomech 45(16):2866–2875. https://doi.org/10.1016/j.jbiomech.2012.08.029
36. Geng X, Lu Y, Liu C, Li W, Yue Z (2019) Fracture characteristic analysis of cellular lattice structures under tensile load. Int J Solids Struct 163:170–177. https://doi.org/10.1016/j.ijsolstr.2019.01.006
37. Ayrilmis N, Nagarajan R, Kuzman MK (2020) Effects of the face/core layer ratio on the mechanical properties of 3d printed wood/polylactic acid (Pla) green biocomposite panels with a gyroid core. Polymers (Basel) 12(12):1–8. https://doi.org/10.3390/polym12122929
38. McGregor DJ, Tawfick S, King WP (2019) Mechanical properties of hexagonal lattice structures fabricated using continuous liquid interface production additive manufacturing. Addit. Manuf 25(September 2018):10–18. https://doi.org/10.1016/j.addma.2018.11.002
39. Nikolaos Kladovasilakis (2021) "Adv Eng Mater - 2021 - Kladovasilakis - Effective mechanical properties of additive manufactured strut-lattice structures .pdf." https://doi.org/10.1002/adem.202100879
40. Fleck NA, Qiu X (2007) The damage tolerance of elastic–brittle, two-dimensional isotropic lattices. J Mech Phys Solids 55(3):562–588. https://doi.org/10.1016/j.jmps.2006.08.004
41. Li P, Wang Z, Petrinic N, Siviour CR (2014) Deformation behaviour of stainless steel microlattice structures by selective laser melting. Mater Sci Eng A 614:116–121. https://doi.org/10.1016/j.msea.2014.07.015
42. Maskery I, Aboulkhair NT, Aremu AO, Tuck CJ, Ashcroft IA (2017) Compressive failure modes and energy absorption in additively manufactured double gyroid lattices. Addit Manuf 16:24–29. https://doi.org/10.1016/j.addma.2017.04.003
43. Nazir A, Jeng J-Y (2020) Buckling behavior of additively manufactured cellular columns: experimental and simulation validation.

Mater Des 186:108349. https://doi.org/10.1016/j.matdes.2019.108349
44. Khan N, Riccio A (2024) A systematic review of design for additive manufacturing of aerospace lattice structures: current trends and future directions. Prog Aerosp Sci 149:101021. https://doi.org/10.1016/j.paerosci.2024.101021
45. A Nazir, AB Arshad, J-Y Jeng (2019) "Buckling and post-buckling behavior of uniform and variable-density lattice columns fabricated using additive manufacturing." https://doi.org/10.3390/ma12213539
46. Latture RM, Rodriguez RX, Holmes LR, Zok FW (2018) Effects of nodal fillets and external boundaries on compressive response of an octet truss. Acta Mater 149:78–87. https://doi.org/10.1016/j.actamat.2017.12.060
47. CH Chuang, J-S Huang (2002) "Effects of solid distribution on the elastic buckling of honeycombs." Int J Mech Sci 44:1429–1443 [Online]. Available: https://api.semanticscholar.org/CorpusID:136939765
48. Simone AE, Gibson LJ (1998) Effects of solid distribution on the stiffness and strength of metallic foams. Acta Mater 46(6):2139–2150. https://doi.org/10.1016/S1359-6454(97)00421-7
49. Wu Y, Yang L (2020) The effect of unit cell size and topology on tensile failure behavior of 2D lattice structures. Int J Mech Sci 170(December 2019):105342. https://doi.org/10.1016/j.ijmecsci.2019.105342
50. Khosravani MR, Anders D, Reinicke T (2023) Effects of post-processing on the fracture behavior of surface-treated 3D-printed parts. CIRP J Manuf Sci Technol 46:148–156. https://doi.org/10.1016/j.cirpj.2023.08.006
51. Khosravani MR, Reinicke T (2020) 3D-printed sensors: current progress and future challenges. Sensors Actuators A Phys 305:111916. https://doi.org/10.1016/j.sna.2020.111916
52. Khosravani MR, Božić Ž, Zolfagharian A, Reinicke T (2022) Failure analysis of 3D-printed PLA components: impact of manufacturing defects and thermal ageing. Eng Fail Anal 136:106214. https://doi.org/10.1016/j.engfailanal.2022.106214
53. Khan T et al (2024) Recent developments in improving the fracture toughness of 3D-printed fiber-reinforced polymer composites. Compos Part B Eng 283:111622. https://doi.org/10.1016/j.compositesb.2024.111622
54. Lyu Q, Lu S (2023) P1. Construction of surface HA/TiO2 coating on porous titanium cages produced by 3D printing and the study of its efficacy in promoting the spinal fusion in a goat model. Spine J 23(9 Supplement):S109. https://doi.org/10.1016/j.spinee.2023.06.226
55. "ASTM D638–14 (2014) Standard test method for tensile properties of plastics, ASTM International, West Conshohocken, PA, 2014,". [Online]. Available: https://www.astm.org/
56. Tymrak BM, Kreiger M, Pearce JM (2014) Mechanical properties of components fabricated with open-source 3-D printers under realistic environmental conditions. Mater Des 58:242–246. https://doi.org/10.1016/j.matdes.2014.02.038
57. Abeykoon C, Sri-Amphorn P, Fernando A (2020) Optimization of fused deposition modeling parameters for improved PLA and ABS 3D printed structures. Int J Light Mater Manuf 3(3):284–297. https://doi.org/10.1016/j.ijlmm.2020.03.003
58. M F A, N A F V S DESHPANDE (2000) "Foam topology bending versus stretching dominated architectures." Acta Mater 49:1035–1040 [Online]. Available: www.elsevier.com/locate/actamat
59. Rajeev A et al (2022) Parametric optimization of corner radius in hexagonal honeycombs under in-plane compression. J Manuf Process 79:35–46. https://doi.org/10.1016/j.jmapro.2022.04.041
60. P Sabine, C Plumpton (1985) Statistics. https://doi.org/10.1007/978-1-349-07668-0